

1
2
3
4
5
6
7
8
9
10
11
12
13
14
15
16
17
18
19
20
21
22
23
24
25
26
27
28
29
30
31
32
33
34
35
36
37
38
39
40
41
42
43
44
45
46
47
48
49
50
51
52
53
54
55
56
57
58
59
60
61
62
63
64
65

Thermodynamic dissection of the interface between HIV-1 gp41 heptad repeats reveals cooperative interactions and allosteric effects.

Samuel Jurado, Mario Cano-Muñoz, Daniel Polo-Megías, Francisco Conejero-Lara* and Bertrand Morel*

Departamento de Química Física, Instituto de Biotecnología e Unidad de Excelencia de Química, Facultad de Ciencias, Universidad de Granada, 18071 Granada, Spain

***Corresponding authors:**

B. Morel; e-mail: bmorel@ugr.es.

F. Conejero-Lara; tel. +34 958 242371; e-mail: conejero@ugr.es.

Abbreviations:

Env, HIV-1 envelope glycoprotein; gp41, glycoprotein subunit 41; gp120, glycoprotein subunit 120; CHR, C-terminal heptad repeat; NHR, N-terminal heptad repeat; CTP, C-terminal pocket; NTP, N-terminal pocket; MP, middle pocket; HP, hydrophobic pocket; CD, circular dichroism spectroscopy; ITC, isothermal titration calorimetry.

Keywords: Fusion inhibitors, calorimetry, peptides, binding affinity, coiled-coil.

1
2 **Highlights**
3
4

- 5 • Targeting only the hydrophobic pocket is not sufficient from the point of view
6 of an inhibitory drug.
7
8
- 9
10 • The number of interaction sites is highly relevant to obtain high affinity.
11
12
- 13 • Binding energy is distributed throughout the NHR-CHR interface.
14
15
- 16 • Allosteric effects are propagated through the NHR coiled-coil structure.
17
18
19
20
21
22
23
24
25
26
27
28
29
30
31
32
33
34
35
36
37
38
39
40
41
42
43
44
45
46
47
48
49
50
51
52
53
54
55
56
57
58
59
60
61
62
63
64
65

Abstract

1
2
3
4 HIV-1 glycoprotein 41 (gp41) mediates fusion between virus and target cells by folding
5 into a fusion active state, in which the C-terminal heptad repeat (CHR) regions associate
6 externally to the N-terminal heptad repeat (NHR) trimer and form a very stable six-helix
7 bundle coiled-coil structure. Therefore, interfering with the NHR-CHR interaction of
8 gp41 is a promising therapeutic approach against HIV-1. However, a full understanding
9 of the molecular and mechanistic details of this interaction is still incomplete.
10

11
12 Here, we use single-chain, chimeric proteins (named covNHR) that reproduce
13 accurately the CHR-NHR interactions to analyze the binding thermodynamics of
14 several peptides with different length from the CHR region. The results indicate that
15 cooperative binding involving two or more pockets of the NHR groove is necessary to
16 obtain relevant affinities and that the binding energy is broadly distributed along the
17 interface, underlining a crucial role of a middle pocket to achieve tight binding. In
18 contrast, targeting only the deep hydrophobic pocket is insufficient to achieve
19 significant affinity. Moreover, calorimetry experiments in combination with limited
20 proteolysis performed using a mutant with occluded binding in the N-terminal pocket
21 reveal the existence of an allosteric communication between the different regions.
22

23
24 This study is the first detailed thermodynamic dissection of the NHR-CHR interaction
25 in gp41 and contributes therefore to a better understanding of HIV fusion. These results
26 are relevant for the development of potential fusion inhibitors.
27
28
29
30
31
32
33
34
35
36
37
38
39
40
41
42
43
44
45
46
47
48
49
50
51
52
53
54
55
56
57
58
59
60
61
62
63
64
65

Introduction

HIV infection continues to be one of the largest pandemics with more than 1 million deaths annually, although modern HAART antiretroviral therapies have helped to reduce the number of deaths. However, in the absence of an effective vaccine, the growing emergence of multi-resistant HIV variants to several of these drugs urges for the development of some new anti-HIV compounds directed against the different stages of the virus life cycle, and in particular against the entry of HIV into the cell.

Considerable efforts to develop HIV therapies have been focused on preventing the cell-virus fusion by blocking the HIV envelope protein (Env) [1-3]. Env is a non-covalently associated trimer of heterodimers of two glycoprotein subunits, gp120 and gp41 playing crucial roles in HIV cell infection [4-6]. The binding of gp120 to CD4 and a co-receptor (CXCR4 or CCR5) triggers a series of large conformational changes within gp41 adopting finally an energetically more favorable conformation, also known as 6-helix-bundle (6HB). This consists in an anti-parallel arrangement of three helical C-terminal heptad repeat (CHR) regions and a central helical trimer of three N-terminal heptad repeat (NHR) regions in a coiled-coil conformation [7, 8]. This process brings the viral and cell membranes into close proximity facilitating fusion. For this reason, the gp41 protein has become a very attractive target for the development of potential HIV-1 inhibitors.

Different molecules able to recognize both NHR and CHR regions of gp41 have been described as fusion inhibitors [3]. They interfere with the 6HB formation and have been classified in two groups according to their specific target region in gp41. Class-1 inhibitors target the hydrophobic grooves exposed by the trimeric coiled-coil of NHR helices. This group is composed of CHR peptide mimics [1, 9-11], artificial D-peptides [12], small compounds [13, 14] and antibodies [15, 16]. On the other side, class-2 inhibitors target the prefusion intermediate by binding to the CHR region. The NHR peptide mimics compared to CHR peptides have a generally lower anti-HIV-1 activity and can inhibit the fusion process only in the micromolar range, compared to the nanomolar range of activity exhibited by the latter. This limited potency may be due to the low solubility and tendency to aggregate of NHR peptides in solution. These problems can be alleviated by engineered protein constructs that imitate exposed trimeric NHR grooves. However, they have certain advantages such as their activity against strains resistant to CHR inhibitors [17, 18]. Despite these promising therapeutic

1 approaches, the CHR peptide T20 (enfuvirtide) is the only FDA-approved HIV fusion
2 inhibitor [9]. Unfortunately, its clinical use has been limited by its short half-life [19]
3 (proteolysis-sensitive and rapid renal filtration) requiring therefore high dosage
4 injections at least twice a day. Moreover, the continuous and expensive treatment
5 generates the appearance of T20-resistant viruses. Nevertheless, such constructs are able
6 to interfere with the formation of the NHR/CHR 6-HB and present potent inhibitory
7 activity against various strains of HIV, demonstrating that both CHR and NHR regions
8 of gp41 continue to be very attractive targets for drug design strategies [20-24].

9 Recently, we have designed, produced and characterized several protein molecules that
10 mimic the structure of the NHR helices trimer of the intermediate state of fusion of
11 gp41 [25, 26]. These proteins, called covNHR, consist of a single polypeptide chain
12 with three helical regions that fold as a trimeric bundle with a structure highly similar to
13 the NHR gp41 region. These proteins are produced recombinantly by expression in *E.*
14 *coli* with good yields, without any post-translational modification. They are also very
15 stable and highly soluble. We have shown that covNHR molecules bind with high
16 affinity to peptides derived from the CHR region of gp41 and neutralize HIV cell
17 infection with high potency (IC₅₀ in the low nanomolar range) for a wide variety of HIV
18 strains and even for T20-resistant variants [26].

19 In our most recent study, we have solved the crystallographic structure of one of these
20 covNHR variants (covNHR-VQ) in complex with the CHR-derived peptide C34 [26].
21 The CHR-NHR binding interface is virtually identical to that observed for various
22 constructs representing the gp41 post-fusion conformation. Therefore, covNHR-VQ
23 protein is a highly accurate mimic of the trimeric NHR coiled-coil, although exposing a
24 single interface for CHR binding. This NHR groove is composed of several sub pockets
25 (Fig. 1a). The most prominent one is the deep hydrophobic pocket (HP) [1], which has
26 been widely used as a target for the discovery of small-molecule inhibitors, short
27 peptides and antibodies. Another important site of interaction occurs at an N-terminal
28 pocket (NTP), where polar CHR and NHR residues establish a dense network of polar
29 interactions and hydrogen bonds mediated by two interfacial water molecules [26].
30 Mutations at this region disrupt this interaction network and are related to the
31 emergence of resistance to CHR peptides. Between these two pockets, we previously
32 identified a shallow middle pocket (MP), on which several aliphatic residues interact
33 [25]. Finally, additional interactions with NHR have been described for CHR residues
34 located N-terminally to the hydrophobic pocket-binding motif [11]. In some available
35
36
37
38
39
40
41
42
43
44
45
46
47
48
49
50
51
52
53
54
55
56
57
58
59
60
61
62
63
64
65

1 X-ray structures, these CHR residues do not maintain the α -helical structure but the
2 chain is directed sideward of the NHR groove with Met626 and Thr627 forming a
3 “hook” structure that hydrophobically caps the HP interaction [27]. However, an
4 additional pocket, C-terminally located to the HP has been defined [28] and the mode in
5 which the N-terminal part of CHR is structured and interacts with this C-terminal
6 pocket (CTP) remains still unclear.
7

8
9
10 Therefore, the NHR-CHR interaction is composed of several important hot spots and
11 the binding energy appears to be broadly distributed along the interface [29]. However,
12 it remains unclear how this binding energy is distributed, how the different hot spots
13 relate to each other and what would be the minimal interaction motif for an effective
14 inhibition. Moreover, a full understanding of the thermodynamic signature of the
15 interaction is still incomplete. Calorimetric analyses of the gp41 NHR-CHR interaction
16 are scarce due to the lack of well-behaved gp41-derived constructs [30-33] and the most
17 accurate and detailed studies are limited to short CHR peptides targeting the
18 hydrophobic pocket [34, 35].
19

20 Because our covNHR proteins are very well behaved and bind the CHR peptides with
21 1:1 stoichiometry, they are particularly amenable for thermodynamic studies of the
22 CHR-NHR interaction. For this reason in this study, we employ the previously
23 described covNHR proteins [26] to perform a detailed thermodynamic dissection of the
24 NHR-CHR interaction. Using isothermal titration calorimetry (ITC) we studied the
25 binding of several different length peptides encompassing every CHR binding motif.
26 Our results increase our understanding about the role of each region in the CHR-NHR
27 binding interface and may aid in the development of future inhibitors.
28
29
30
31
32
33
34
35
36
37
38
39
40
41
42

43 **Materials and Methods**

44 *Protein and peptide samples*

45
46
47 The DNA encoding the covNHR protein sequences was synthesized by Thermofisher
48 Scientific (Waltham, USA). To facilitate purification by Ni-Sepharose affinity
49 chromatography, the protein sequences were histidine tagged at the C-terminus with the
50 sequence GGGGSHHHHHH. The covNHR proteins were produced by overexpression
51 in *E. coli*, as described previously [25]. Synthetic CHR peptides, both N-acetylated and
52 C-amidated, were acquired from Genecust (Luxembourg), with a purity >95%. Protein
53 and peptide concentrations were determined by UV absorption measurements at 280 nm
54
55
56
57
58
59
60
61
62
63
64
65

1
2
3
4
5
6
7
8
9
10
11
12
13
14
15
16
17
18
19
20
21
22
23
24
25
26
27
28
29
30
31
32
33
34
35
36
37
38
39
40
41
42
43
44
45
46
47
48
49
50
51
52
53
54
55
56
57
58
59
60
61
62
63
64
65

with extinction coefficients calculated according to their respective amino acid sequences with the ExPasy ProtParam server (<https://web.expasy.org/protparam/>) [36]. In the case of peptide E14L, devoid of aromatic groups, the concentration was determined by measurement of the absorbance at 205 nm using an extinction coefficient of $38540 \text{ M}^{-1} \cdot \text{cm}^{-1}$ calculated with <https://spin.niddk.nih.gov/clore/> [37].

Circular dichroism

Circular dichroism (CD) experiments were performed on a Jasco J-715 spectropolarimeter (Jasco, Tokyo, Japan) equipped with Peltier-thermostatic cell holder. Measurements of the far-UV CD spectra (250–200 nm) were made with a 1 mm path length quartz cuvette at a protein concentration of $\sim 15 \mu\text{M}$ using a bandwidth of 1 nm, a scan rate of 100 nm/min and a response time of 1 s. The resulting spectra were usually the average of five scans. Near-UV CD spectra (340–250 nm) were measured at a protein concentration of $\sim 40 \mu\text{M}$ using a 5 mm cuvette and were typically the average of 20 scans. The interaction experiments were carried at a 1:2 molar ratio between the protein and each CHR peptide. Each spectrum was corrected by baseline subtraction using the blank spectrum obtained with the buffer and finally the CD signal was normalized to molar ellipticity ($[\theta]$, in $\text{deg} \cdot \text{dmol}^{-1} \cdot \text{cm}^2$).

Isothermal titration calorimetry

ITC measurements were carried out in a Microcal VP-ITC calorimeter (Malvern Instruments, Worcestershire, UK). The protein solutions were typically titrated with 25 injections of $5 \mu\text{L}$ peptide solution using an interval of 480 sec. Concentrations of the protein used for the titrations were in the range of $10 \mu\text{M}$, while the ligands in the syringe were around $300 \mu\text{M}$ depending on their solubilities. The experiments were carried out in 50 mM phosphate buffer, pH 7.4 at 25°C unless specifically stated. As a blank, an independent experiment with only buffer in the calorimeter's cell was performed with the same peptide solution to determine the corresponding heats of dilution. The experimental thermograms were baseline corrected and the peaks were integrated to determine the heats produced by each ligand injection. Finally, each heat was normalized per mole of added ligand. The resulting binding isotherms were fitted using a binding model of independent sites, allowing the determination of the binding constant, K_b , the binding enthalpy, ΔH_b , and the binding stoichiometry, n , for each

1 interaction. From these values, the Gibbs energy and entropy of binding could be
2 derived as $\Delta G_b = -RT \cdot \ln K_b$ and $T \cdot \Delta S_b = \Delta H_b - \Delta G_b$. For low affinity peptides we
3 carried out displacement experiments, in which the protein was mixed in the
4 calorimetric cell with the low-affinity peptide at several molar ratios and the mixtures
5 were titrated with a previously characterized, high-affinity peptide competing for the
6 same interactions. The data were analyzed as described previously [38].
7
8
9
10

11 *Limited proteolysis*

12 Proteolysis experiments were carried out using thermolysin as protease (Sigma, St
13 Louis, MO) in 50 mM HEPES, 100 mM NaCl, 5 mM CaCl₂ pH 7.2. Aliquots of the
14 covNHR proteins at 30 μ M concentration, previously dialyzed in the buffer and
15 equilibrated at the desired temperature, were mixed with thermolysin at 500:1
16 protein:protease ratio and incubated in a thermoblock at 20°C. The reaction was stopped
17 at different times by adding EDTA to reach 20 mM concentration and the sample
18 aliquots were immediately frozen. The samples were analyzed by SDS-PAGE in
19 Tris/Tricine buffers and by HPLC coupled to ESI-MS in a WATERS LCT Premier XE
20 instrument equipped with a time-of-flight analyzer. Fragments were identified using the
21 ExPasy PeptFind tool (<https://www.expasy.org/>).
22
23
24
25
26
27
28
29
30
31
32
33

34 **Results**

35 *Description of the CHR peptides*

36 In this study, we evaluated the capacity of covNHR-VQ to bind several synthetic
37 peptides encompassing different CHR segments of gp41, namely CHR-628–661 (C34),
38 CHR-638–661 (Y24L), CHR-628–651 (W24N), CHR-628–640 (W13S), CHR-616–640
39 (N25S), CHR-638–651 (Y14N), CHR-648–661 (E14L), CHR-616–651 (N36N) (Fig.
40 1c).
41
42
43
44
45
46
47
48

49 The peptides could be classified according to the number of NHR pockets covered by
50 their binding. C34 and N36N are expected to interact with three pockets of covNHR-
51 VQ, W24N, N25S and Y24L would bind to two pockets, and finally, the shortest
52 peptides are susceptible to bind only to a single pocket: W13S with the HP, the Y14N
53 with the MP, and the E14L with the NTP. The different regions of interaction are
54 underlined in different colors in Figure 1c. To avoid the influence of terminal charges,
55 the peptides were N-acetylated and C-amidated. Moreover, the sequences of peptides
56
57
58
59
60
61
62
63
64
65

1 targeted to adjacent pockets were chosen to overlap by three or four residues in order to
2 reduce helix end-fraying effects.
3
4

5 *Binding mode of CHR peptides* 6

7 To characterize the interaction between covNHR-VQ and the different peptides, we
8 compared the far-UV CD spectra of the protein-peptide mixtures with those of the free
9 molecules (Fig. 2a-b). In isolation, the different CHR peptides exhibit similar spectra
10 typical of unfolded polypeptides. Therefore, since bound peptides should acquire α -
11 helical structure, binding is indicated by an increase in the negative molar ellipticity
12 compared to the sum of the individual spectra of the free molecules.
13
14
15
16

17 A significant increase in negative molar ellipticity was clearly observed with W24N,
18 Y24L, N25S, N36N and C34, indicating therefore binding to covNHR-VQ. The change
19 in ellipticity increases gradually with the number of amino acids (Fig. 2a). On the other
20 hand, W13S, E14L and Y14N, targeting single pockets, do not seem to bind
21 significantly to the protein because the molar ellipticity does not increase (Fig. 2b).
22
23
24
25
26

27 Subsequently, near-UV CD spectra of the protein-peptide mixtures were also measured.
28 Our previous studies have shown that the stacking of CHR tryptophan side chains onto
29 the hydrophobic pocket of covNHR proteins results in a characteristic negative
30 ellipticity band centered at 293 nm [25, 26]. CovNHR-VQ presents a weak negative
31 band at around 280 nm corresponding to the tryptophan side chain present in the
32 hydrophobic pocket. Upon mixing with C34, N25S, N36N or W24N, the Near-UV CD
33 spectra exhibit intense shifted negative ellipticity bands indicating interaction of the
34 CHR peptides with the hydrophobic pocket of covNHR-VQ (Fig. 2c). While binding of
35 W13S was expected, the mixture with this peptide does not present such characteristic
36 signal. However, the region of the spectrum between 277-260 nm is affected in presence
37 of W13S (Fig. 2d), indicating a change in the environment of the protein aromatic
38 amino acids and suggesting therefore a possible weak interaction of this peptide. The
39 Near-UV CD spectra are not affected by the presence of Y14N, E14L and Y24L (Fig.
40 2d), as expected since these peptides do not bind to the hydrophobic pocket of covNHR-
41 VQ and E14L does not have aromatic residues.
42
43
44
45
46
47
48
49
50
51
52
53
54
55

56 *Isothermal Titration Calorimetry* 57

58 In a recent study, we already characterized the thermodynamics of binding of C34 to
59 covNHR-VQ by a combination of ITC and DSC [26]. CovNHR-VQ has an
60
61
62
63
64
65

1
2
3
4
5
6
7
8
9
10
11
12
13
14
15
16
17
18
19
20
21
22
23
24
25
26
27
28
29
30
31
32
33
34
35
36
37
38
39
40
41
42
43
44
45
46
47
48
49
50
51
52
53
54
55
56
57
58
59
60
61
62
63
64
65

outstandingly high affinity for C34 ($K_d < 0.1$ pM) mainly driven by a highly favorable binding enthalpy, consequence of a combination of an extensive binding interface covering three pockets, significant structural tightening accompanying complex formation and participation of interfacial water molecules at the NTP. Here, we intend first to thermodynamically dissect this interaction by analyzing shorter peptides targeted to the pockets' subsets using ITC.

The W24N peptide contains only the MP and HP binding motifs. The C-terminus of this peptide ends just before the NTP motif, associated with T20 resistance (Fig. 1). W24N binds to covNHR-VQ with 1:1 stoichiometry, a considerable negative binding enthalpy and moderately high affinity ($K_d = 80 \pm 7$ nM at 25°C) (Fig. 3a and Table 1), corroborating the CD experiments. Its affinity is very similar to that obtained with Y24L peptide that spans the NTP and MP binding motifs ($K_d = 90 \pm 7$ nM at 25°C) (Table 1 and Fig. S1A) and also reported in our previous article ($K_d = 81 \pm 15$ nM) [26]. However, Y24L possesses much higher binding enthalpy than W24N, likely as a result of a more polar character of the interactions at the NTP.

Binding heat capacities of W24N and Y24L were determined by measuring the binding enthalpy at several temperatures. The values are respectively -1.9 ± 0.1 kJ·K⁻¹·mol⁻¹ and -1.6 ± 0.1 kJ·K⁻¹·mol⁻¹ (Table 1). It is remarkable that, despite each of these peptides covers two of the three pockets bound by C34, the sum of their binding enthalpies is significantly lower than that of C34 (-126 kJ·mol⁻¹ at 25°C), and the sum of their ΔC_p values is approximately equivalent to that obtained for the complex covNHR-VQ:C34 ($\Delta C_p = -3.6 \pm 0.4$ kJ·K⁻¹·mol⁻¹) [26].

Subsequently, to investigate the binding of CHR motifs to individual NHR pockets we studied three different peptides (W13S, Y14N and E14L) (Fig. 1). The W13S peptide contains the hydrophobic residues that have been described as essential for the interaction with the NHR pocket, namely, Trp628, Trp631 and Ile635 (Fig. 1). As expected from the CD experiments, W13S showed very weak binding in direct ITC titration experiments. Therefore, displacement experiments were carried out by titrating several mixtures of covNHR-VQ/W13S with W24N (Fig. S2A). This experiment confirmed a weak binding with a high dissociation constant ($K_d = 330 \pm 150$ μM) and relatively low binding enthalpy, explaining the weak differences observed in the CD experiments. Similar ITC experiments were performed with Y14N and E14L that contain the CHR motifs directed to the MP and NTP respectively. However, no significant binding was detected for any of these peptides, even in displacement

1 experiments (Fig. S2B). These results indicate that one-site specific interactions at the
2 HP, MP and NTP regions do not provide individually a crucial contribution to the
3 binding energetics and therefore high binding affinity is only achieved by multiple
4 cooperative interactions, involving at least two pockets, with the MP playing a key role.
5
6

7
8
9 It has been previously described that residues upstream of the pocket-binding motif
10 strongly contribute to the CHR-NHR interaction, are essential for viral infectivity and
11 crucial for inhibition by peptides [11, 27, 28]. Therefore, we investigated the binding of
12 CHR peptides including the ⁶²¹QIWNNMT⁶²⁷ motif, upstream to C34. Previous
13 attempts to perform ITC experiments with Q32Q (CP32 in the literature, residues 621-
14 652) and Q20S (residues 621-640) were impaired by low solubility and self-association
15 of the peptides, yielding unreliable ITC data (results not shown). To obtain more
16 soluble peptides, we added 5 additional upstream residues, including several polar and
17 charged residues. Two peptides were studied: N36N and N25S, encompassing the
18 binding motifs of the CTP and one or two additional pockets (HP and MP) (Fig. 1c).
19
20

21
22
23
24
25
26
27 The N36N peptide binds to covNHR-VQ with a dissociation constant of 63 ± 12 nM
28 (Table 1, Fig. S1B). This affinity is only slightly higher than that of the shorter peptide
29 W24N interacting with only the HP and MP pockets. Also, the binding enthalpy of
30 N36N and W24N differ in only 2 kJ mol^{-1} . Accordingly, the residues upstream of the
31 pocket-binding motif do not appear to contribute to a tighter interaction of the N36N
32 peptide compared to the shorter W24N. This is in contrast with the extremely high
33 affinity observed for C34, which has a similar length and also targets three pockets [26].
34 This is in good agreement with the lower gain of ellipticity of covNHR-VQ/N36N than
35 that observed for covNHR-VQ/C34 [26] (Fig. 2a).
36
37

38
39
40
41
42
43 We also assayed a shorter peptide (N25S), which does not include CHR residues
44 interacting with the MP (Fig. 1c). This peptide tends however to aggregate at
45 concentrations above 200-250 μM , precluding a successful direct ITC study. For this
46 reason, displacement experiments with W24N were carried out (Fig. 3b). A relatively
47 high dissociation constant $3.0 \pm 0.2 \mu\text{M}$ was obtained for N25S. The negative binding
48 enthalpy and heat capacity were relatively low in magnitude compared to the other
49 peptides of similar length, also targeting two pockets, but the parameters still indicate
50 considerable interactions. As a result, compared to the W13S peptide the binding
51 affinity increases by two orders of magnitude. This indicates that addition of the CTP
52
53
54
55
56
57
58
59
60
61
62
63
64
65

1 binding motif to the HP motif enhances cooperatively the interaction. Strikingly, a
2 similar affinity increase effect from the CTP motif is not observed for the N36N peptide
3 compared to the W24N peptide. This suggests that the binding mode of the CTP motif
4 depends on whether the MP pocket is occupied or not. This highlights an important role
5 of the MP in modulating the CHR-NHR interaction.
6
7

8 From these results, it emerges that the CHR-NHR interaction can be very tight as a
9 result of a strong cooperative communication between pockets but at the same time it
10 can be flexible to partially compensate local disruption of the interaction at specific
11 pockets.
12
13
14
15
16
17

18 *Binding properties of CHR peptides to covNHR-ER: A possible inter-domain*
19 *communication.*
20

21 To study further these cooperative effects, we used the double mutant covNHR-ER,
22 which was described in our last paper [26]. This variant serves as a ‘knockout’ mutant,
23 in which binding at the NTP is completely abolished by two mutations V10E and
24 Q123R.
25
26
27
28

29 Despite the local impairment of interactions at the NTP, we have previously shown that
30 covNHR-ER maintains a low nanomolar affinity for C34 [26], with binding parameters
31 that indicate tight interactions at HP and MP (Table 1). To further investigate any
32 possible long-range effects in the peptide binding produced by the local modifications at
33 the NTP, we have studied the interactions between covNHR-ER and three CHR
34 peptides that do not have the motif interacting with the NTP. Therefore, ITC
35 experiments were performed with W13S that binds to HP exclusively; W24N that binds
36 to HP and MP; and N36N, which binds to CTP, HP and MP (Fig. 1c).
37
38
39
40
41
42
43

44 CovNHR-ER binds the W24N peptide with affinity in the tens of nanomolar range,
45 although 2.5 times tighter than covNHR-VQ (Table 1). We could also notice that there
46 is a significant increase in the negative binding enthalpy of -14 kJ mol^{-1} for this peptide
47 produced by the ER mutations. The binding parameters between W13S and covNHR-
48 ER were obtained from displacement experiments similar to those described for
49 covNHR-VQ. These experiments yielded a slightly lower dissociation constant ($K_d =$
50 $290 \pm 80 \mu\text{M}$) for covNHR-ER compared to covNHR-VQ ($K_d = 330 \pm 150 \mu\text{M}$) but,
51 interestingly, this short peptide also has a more negative binding enthalpy for covNHR-
52 ER compared to covNHR-VQ. Similar results were obtained for the N36N peptide,
53 once again with a slightly smaller K_d value and a more negative binding enthalpy. Since
54
55
56
57
58
59
60
61
62
63
64
65

1 the three peptides share only the HP binding motif, we can ascribe the long-range effect
2 produced by the mutations to this particular pocket.

3 To investigate any conformational changes that may be related to this long-range
4 allosteric cooperative effect, we carried out limited proteolysis experiments comparing
5 covNHR-ER and covNHR-VQ under identical conditions. The results are summarized
6 in the Supplementary Information (Fig. S3). The most flexible parts in both proteins are
7 the loops and the C-terminal end, which undergo rapid cleavage within the first 30 min
8 generating fragments corresponding to one or two complete helices that persist during
9 the full experiment (240 min), likely due to their self-association. However, after 180
10 min of proteolysis covNHR-VQ undergoes slower cleavage at Ile9, Leu106 and Ile120,
11 whereas covNHR-ER is cleaved only at Leu106 and Leu117. This indicates a higher
12 local stability of the NTP region in covNHR-ER, likely produced by a stabilizing salt
13 bridge between the Glu10 and Arg123 side chains. This local structural change that
14 disrupts completely the binding at the T20-resistance motif also appears to cause a long-
15 range restructuring at the HP favoring a tighter interaction.

16 These results confirm the existence of long-range allosteric effects along the coiled-coil
17 structure of the covNHR proteins that modulate the CHR-NHR interaction.

31 Discussion

32 Most of the current knowledge about NHR-CHR interaction comes from mutational
33 effect observations but detailed structural and thermodynamic studies about the binding
34 interface are still very scarce. In this work, we take the advantage of the fact that the
35 covNHR proteins are extremely accurate mimics of an exposed NHR surface and
36 constitute useful models to investigate the interactions between CHR and NHR in gp41
37 that drive HIV-1 fusion. Such results provide significant insight into the forces that
38 drive HIV-1 fusion, inhibition by peptides and acquisition of resistance.

39 The thermodynamic magnitudes obtained from this extensive calorimetric analysis are
40 collected in Table 1 and summarized in Figure 4. It was shown in our previous study
41 that the extremely favorable binding enthalpy for the C34 peptide to covNHR-VQ
42 results from a vast binding interface, conformational tightening accompanying binding
43 and participation of interfacial water molecules [26]. In this study, the thermodynamic
44 signatures for the peptides binding share to different extents similar enthalpy-entropy
45 compensation being characteristic of binding coupled to folding. However, there are
46
47
48
49
50
51
52
53
54
55
56
57
58
59
60
61
62
63
64
65

1
2 some marked differences between the peptides in the binding enthalpy and also in the
3 binding entropy terms, depending on the dominant interaction site at NHR.
4

5 *Contributions to the NHR-CHR interaction. Thermodynamic signature.*
6

7 As described in the Introduction, the NHR binding interface for the CHR peptides can
8 be divided in four regions or pockets. The interaction of the W13S peptide at the
9 prominent HP accounts for merely -20 kJ mol^{-1} of binding energy (Fig. 4a). The
10 binding is driven by equally favorable, small entropy and enthalpy contributions (about
11 -10 kJ mol^{-1} each). The positive binding entropy is most probably due to a large burial
12 of hydrophobic surface in the pocket and may also suggest a relatively mobile
13 conformation of the bound peptide. The small negative binding enthalpy is in agreement
14 with the formation of few hydrogen bonds within the W13S backbone due to the short
15 peptide length. Addition of 11 downstream residues (W24N peptide), interacting with
16 the MP approximately doubles the binding Gibbs energy with an increase in negative
17 binding enthalpy of about -40 kJ mol^{-1} . This indicates an increased contribution of
18 hydrogen bonds relative to the hydrophobic interactions and a larger decrease in
19 conformational entropy due to a more ordered bound peptide conformation.
20

21 We have shown in our previous paper that the presence of the last ten residues in the
22 full C34 peptide produces a very strong increase in both the negative enthalpy and
23 entropy of binding. These C-terminal residues of C34 are involved in a dense network
24 of water-mediated intra- and intermolecular hydrogen bond interactions at the NTP. In
25 spite of these prominent features, it is quite unlikely that all the energy gain can be
26 ascribed to this interaction and other effects including changes in solvation, dynamics
27 and cooperative effects play likely a part in these increases. In fact, the binding Gibbs
28 energy of Y24L to covNHR-VQ, whose binding covers the NTP and MP, amounts only
29 -40 kJ mol^{-1} , which is just above half of that of the reported one for C34 [26]. The
30 binding enthalpy of this peptide is -63 kJ mol^{-1} , about a half that of C34. For similar
31 reasons, the binding energy and enthalpy differences between these two peptides cannot
32 be attributed exclusively to interactions at the HP. These results clearly demonstrate that
33 the binding enthalpies and energies for each pocket are not additive magnitudes and that
34 there are cooperative effects between domains that propagate the binding energy
35 throughout the whole interface.
36

37 It might be argued that the non-additive nature of the binding energy could be attributed
38 to an avidity effect due a lower translational-rotational entropy cost in the binding of a
39
40
41
42
43
44
45
46
47
48
49
50
51
52
53
54
55
56
57
58
59
60
61
62
63
64
65

1 larger peptide compared to its fragments. We must emphasize however that we are
2 reporting standard Gibbs energies of binding (at 1M standard concentration). At these
3 unrealistically high concentrations the rotational-translational effect of tethering two
4 interacting fragments to form a larger ligand on the binding energies was estimated
5 practically negligible [39]. Moreover, Zhou and Gilson [40] calculated the effect of
6 tethering two ligands binding to adjacent sites with a polypeptide linker on the binding
7 Gibbs energies as $\Delta G_{12} = \Delta G_1 + \Delta G_2 - RT \cdot \ln P(r)$, where ΔG_1 , ΔG_2 and ΔG_{12} are the
8 respective binding energies of the two fragments and the tethered ligand, and $P(r)$ is the
9 effective concentration of the second fragment in the tethered ligand, once the first
10 fragment is bound to its site. With flexible linkers the calculated effective concentration
11 is in the mM range and approaches to the molar range for short and rigid linkers. This
12 indicates that at the standard condition the entropic effect of tethering ligands binding to
13 adjacent sites is negligible or to slightly increase the binding energy, relative to the sum
14 of the binding energies of the individual fragments. Therefore, the large decreases in
15 binding Gibbs energy observed here for peptides targeting multiple pockets can only be
16 attributed to cooperative effects. Moreover, the non-additive binding enthalpies also
17 support this conclusion.

18 A previous study performed with isoforms and mutants of a potent CHR-derived
19 peptide, called T-2635 [41], has reported similar conclusions based on the differences in
20 melting temperatures of the complex with N36 [29]. These results may explain why it
21 has proven difficult to identify small molecules with high antiviral potency despite the
22 remarkable amount of work focused mainly on the study of small aromatic and
23 hydrophobic molecules capable of interacting with the HP [42-45]. Our results suggest
24 that achieving relevant affinities by targeting specifically the HP is a highly complicated
25 task and that addition of other contact regions such as the MP is necessary to reduce the
26 dissociation constant to nM values.

27 Binding to the HP can also be enhanced by addition of residues targeting the CTP, as
28 demonstrated by the results with N25S. However, the differences in binding parameters
29 between N25S and W13S do not match those between N36N and W24N. This implies
30 that the CTP binding motif adopts different conformation in N25S and N36N peptides
31 and suggests some type of antagonism between binding at the MP and at the CTP,
32 which may explain why most residues of the ⁶²¹QIWNNMT⁶²⁷ motif of peptide CP32
33 do not contact the CTP in the complex with T21 but they form a “hook” interrupting the
34 helix [27].

1
2
3
4
5
6
7
8
9
10
11
12
13
14
15
16
17
18
19
20
21
22
23
24
25
26
27
28
29
30
31
32
33
34
35
36
37
38
39
40
41
42
43
44
45
46
47
48
49
50
51
52
53
54
55
56
57
58
59
60
61
62
63
64
65

Additional evidence for the existence of long-range cooperative effects in the NHR-CHR interaction arises from the comparison of the binding results between covNHR-VQ and covNHR-ER using CHR peptides deprived of residues interacting with the NTP. Limited proteolysis indicates a significant conformational flexibility at the NTP pocket region in covNHR-VQ, which is locally stabilized by the V10E and Q123R mutations in covNHR-ER. More favorable binding enthalpies and slightly increased affinities were obtained with the later mutant for the three different peptides (Fig. 4d-f). This implies that the local energy perturbation produced by the mutations at the NTP is propagated more than 30 Å to the HP. This effect complies with a general concept of allostery described elsewhere [46] and therefore demonstrates an allosteric behavior within the NHR coiled coil.

The picture emerging from these results is that the NHR surface is highly flexible and adaptable to interact with different available CHR motifs. In this adaptability, the MP appears to play a central role, promoting high affinity with any or both of the HP and NTP and affecting the interactions at the CTP. These results may be important in the mechanism of fusion, where different CHR regions may become accessible during different phases of the process, or in the development of resistance against fusion inhibitors, in which binding at specific sites of the interface becomes impaired and binding affinity would need to be displaced to other regions of the NHR to maintain significant infectivity.

Conclusion

In this study, we have reported a complete thermodynamic dissection of the interaction between the CHR and NHR regions of the gp41 ectodomain. We have observed that the binding energy is broadly but unevenly distributed along the interface. Peptides targeting a single pocket do not show a relevant affinity and high affinity can only be achieved by targeting at least two binding pockets. Accordingly strong binding cooperativity between the different pockets is observed and allows the development of an extremely high binding affinity. However, removing any of the pocket binding motifs by peptide truncation reduces affinity by five to six orders of magnitude. Moreover, we demonstrate the existence of long-range allosteric effects through the NHR structure, which may be relevant to modulate CHR-NHR interactions in response to mutations and inhibitors.

1 Our results help to understand the forces that drive HIV fusion and are of special
2 interest in the development of an inhibitory drug.
3
4

5 **Acknowledgements**

6
7
8

9 This research was funded by grant BIO2016-76640-R from the Spanish Ministry of
10 Economy and Competitiveness and by the European Fund for Research and
11 Development from the European Union.
12
13
14
15

16 **References**

17
18
19

- 20 1. Chan, D. C., C. T. Chutkowski, and P. S. Kim. 1998. Evidence that a prominent
21 cavity in the coiled coil of HIV type 1 gp41 is an attractive drug target.
22 *Proceedings of the National Academy of Sciences of the United States of*
23 *America* 95:15613-15617.
- 24 2. Eckert, D. M., and P. S. Kim. 2001. Mechanisms of viral membrane fusion and
25 its inhibition. *Annual review of biochemistry* 70:777-810.
- 26 3. Yi, H. A., B. C. Fochtman, R. C. Rizzo, and A. Jacobs. 2016. Inhibition of HIV
27 Entry by Targeting the Envelope Transmembrane Subunit gp41. *Current HIV*
28 *research* 14:283-294.
- 29 4. White, T. A., A. Bartesaghi, M. J. Borgnia, J. R. Meyerson, M. J. de la Cruz, J.
30 W. Bess, R. Nandwani, J. A. Hoxie, J. D. Lifson, J. L. Milne, and S.
31 Subramaniam. 2010. Molecular architectures of trimeric SIV and HIV-1
32 envelope glycoproteins on intact viruses: strain-dependent variation in
33 quaternary structure. *PLoS pathogens* 6:e1001249.
- 34 5. Ward, A. B., and I. A. Wilson. 2017. The HIV-1 envelope glycoprotein
35 structure: nailing down a moving target. *Immunological reviews* 275:21-32.
- 36 6. Munro, J. B., and W. Mothes. 2015. Structure and Dynamics of the Native HIV-
37 1 Env Trimer. *Journal of virology* 89:5752-5755.
- 38 7. Chan, D. C., D. Fass, J. M. Berger, and P. S. Kim. 1997. Core structure of gp41
39 from the HIV envelope glycoprotein. *Cell* 89:263-273.
- 40 8. Weissenhorn, W., A. Dessen, S. C. Harrison, J. J. Skehel, and D. C. Wiley.
41 1997. Atomic structure of the ectodomain from HIV-1 gp41. *Nature* 387:426-
42 430.
- 43 9. Kilby, J. M., S. Hopkins, T. M. Venetta, B. DiMassimo, G. A. Cloud, J. Y. Lee,
44 L. Alldredge, E. Hunter, D. Lambert, D. Bolognesi, T. Matthews, M. R.
45 Johnson, M. A. Nowak, G. M. Shaw, and M. S. Saag. 1998. Potent suppression
46 of HIV-1 replication in humans by T-20, a peptide inhibitor of gp41-mediated
47 virus entry. *Nature medicine* 4:1302-1307.
- 48 10. Eron, J. J., R. M. Gulick, J. A. Bartlett, T. Merigan, R. Arduino, J. M. Kilby, B.
49 Yangco, A. Diers, C. Drobnes, R. DeMasi, M. Greenberg, T. Melby, C.
50 Raskino, P. Rusnak, Y. Zhang, R. Spence, and G. D. Miralles. 2004. Short-term
51 safety and antiretroviral activity of T-1249, a second-generation fusion inhibitor
52 of HIV. *The Journal of infectious diseases* 189:1075-1083.
53
54
55
56
57
58
59
60
61
62
63
64
65

11. He, Y., J. Cheng, J. Li, Z. Qi, H. Lu, M. Dong, S. Jiang, and Q. Dai. 2008. Identification of a critical motif for the human immunodeficiency virus type 1 (HIV-1) gp41 core structure: implications for designing novel anti-HIV fusion inhibitors. *Journal of virology* 82:6349-6358.
12. Welch, B. D., A. P. VanDemark, A. Heroux, C. P. Hill, and M. S. Kay. 2007. Potent D-peptide inhibitors of HIV-1 entry. *Proceedings of the National Academy of Sciences of the United States of America* 104:16828-16833.
13. Frey, G., S. Rits-Volloch, X.-Q. Zhang, R. T. Schooley, B. Chen, and S. C. Harrison. 2006. Small molecules that bind the inner core of gp41 and inhibit HIV envelope-mediated fusion. *Proceedings of the National Academy of Sciences of the United States of America* 103:13938-13943.
14. Lu, L., F. Yu, L. Cai, A. K. Debnath, and S. Jiang. 2016. Development of Small-molecule HIV Entry Inhibitors Specifically Targeting gp120 or gp41. *Current topics in medicinal chemistry* 16:1074-1090.
15. Miller, M. D., R. Geleziunas, E. Bianchi, S. Lennard, R. Hrin, H. Zhang, M. Lu, Z. An, P. Ingallinella, M. Finotto, M. Mattu, A. C. Finnefrock, D. Bramhill, J. Cook, D. M. Eckert, R. Hampton, M. Patel, S. Jarantow, J. Joyce, G. Ciliberto, R. Cortese, P. Lu, W. Strohl, W. Schleif, M. McElhaugh, S. Lane, C. Lloyd, D. Lowe, J. Osbourn, T. Vaughan, E. Emini, G. Barbato, P. S. Kim, D. J. Hazuda, J. W. Shiver, and A. Pessi. 2005. A human monoclonal antibody neutralizes diverse HIV-1 isolates by binding a critical gp41 epitope. *Proceedings of the National Academy of Sciences of the United States of America* 102:14759-14764.
16. Sabin, C., D. Corti, V. Buzon, M. S. Seaman, D. Lutje Hulsik, A. Hinz, F. Vanzetta, G. Agatic, C. Silacci, L. Mainetti, G. Scarlatti, F. Sallusto, R. Weiss, A. Lanzavecchia, and W. Weissenhorn. 2010. Crystal structure and size-dependent neutralization properties of HK20, a human monoclonal antibody binding to the highly conserved heptad repeat 1 of gp41. *PLoS pathogens* 6:e1001195.
17. Eckert, D. M., and P. S. Kim. 2001. Design of potent inhibitors of HIV-1 entry from the gp41 N-peptide region. *Proceedings of the National Academy of Sciences of the United States of America* 98:11187-11192.
18. Root, M. J., M. S. Kay, and P. S. Kim. 2001. Protein design of an HIV-1 entry inhibitor. *Science* 291:884-888.
19. Poveda, E., V. Briz, and V. Soriano. 2005. Enfuvirtide, the first fusion inhibitor to treat HIV infection. *AIDS reviews* 7:139-147.
20. He, Y. 2013. Synthesized peptide inhibitors of HIV-1 gp41-dependent membrane fusion. *Curr Pharm Des* 19:1800-1809.
21. Xiong, S., P. Borrego, X. Ding, Y. Zhu, A. Martins, H. Chong, N. Taveira, and Y. He. 2017. A Helical Short-Peptide Fusion Inhibitor with Highly Potent Activity against Human Immunodeficiency Virus Type 1 (HIV-1), HIV-2, and Simian Immunodeficiency Virus. *Journal of virology* 91.
22. Chong, H., X. Yao, Z. Qiu, J. Sun, Y. Qiao, M. Zhang, M. Wang, S. Cui, and Y. He. 2014. The M-T hook structure increases the potency of HIV-1 fusion inhibitor sifuvirtide and overcomes drug resistance. *The Journal of antimicrobial chemotherapy* 69:2759-2769.
23. Xu, W., J. Pu, S. Su, C. Hua, X. Su, Q. Wang, S. Jiang, and L. Lu. 2019. Revisiting the mechanism of enfuvirtide and designing an analog with improved fusion inhibitory activity by targeting triple sites in gp41. *AIDS* 33:1545-1555.

- 1 24. Zhang, X., X. Ding, Y. Zhu, H. Chong, S. Cui, J. He, X. Wang, and Y. He.
2 2019. Structural and functional characterization of HIV-1 cell fusion inhibitor
3 T20. *AIDS* 33:1-11.
- 4 25. Crespillo, S., A. Camara-Artigas, S. Casares, B. Morel, E. S. Cobos, P. L.
5 Mateo, N. Mouz, C. E. Martin, M. G. Roger, R. El Habib, B. Su, C. Moog, and
6 F. Conejero-Lara. 2014. Single-chain protein mimetics of the N-terminal heptad-
7 repeat region of gp41 with potential as anti-HIV-1 drugs. *Proceedings of the*
8 *National Academy of Sciences of the United States of America* 111:18207-
9 18212.
- 10 26. Jurado, S., M. Cano-Munoz, B. Morel, S. Standoli, E. Santarossa, C. Moog, S.
11 Schmidt, G. Laumond, A. Camara-Artigas, and F. Conejero-Lara. 2019.
12 Structural and Thermodynamic Analysis of HIV-1 Fusion Inhibition Using
13 Small gp41 Mimetic Proteins. *Journal of molecular biology* 431:3091-3106.
- 14 27. Chong, H., X. Yao, Z. Qiu, B. Qin, R. Han, S. Waltersperger, M. Wang, S. Cui,
15 and Y. He. 2012. Discovery of critical residues for viral entry and inhibition
16 through structural Insight of HIV-1 fusion inhibitor CP621-652. *The Journal of*
17 *biological chemistry* 287:20281-20289.
- 18 28. Qiu, Z., H. Chong, X. Yao, Y. Su, S. Cui, and Y. He. 2015. Identification and
19 characterization of a subpocket on the N-trimer of HIV-1 Gp41: implication for
20 viral entry and drug target. *AIDS* 29:1015-1024.
- 21 29. Johnson, L. M., W. S. Horne, and S. H. Gellman. 2011. Broad distribution of
22 energetically important contacts across an extended protein interface. *Journal of*
23 *the American Chemical Society* 133:10038-10041.
- 24 30. He, Y. X., S. W. Liu, W. G. Jing, H. Lu, D. M. Cai, D. J. Chin, A. K. Debnath,
25 F. Kirchhoff, and S. B. Jiang. 2007. Conserved residue Lys(574) in the cavity of
26 HIV-1 gp41 coiled-coil domain is critical for six-helix bundle stability and virus
27 entry. *The Journal of biological chemistry* 282:25631-25639.
- 28 31. Leung, M. Y., and F. S. Cohen. 2011. Increasing hydrophobicity of residues in
29 an anti-HIV-1 Env peptide synergistically improves potency. *Biophysical*
30 *journal* 100:1960-1968.
- 31 32. Geng, X., Z. Liu, D. Yu, B. Qin, Y. Zhu, S. Cui, H. Chong, and Y. He. 2019.
32 Conserved Residue Asn-145 in the C-Terminal Heptad Repeat Region of HIV-1
33 gp41 is Critical for Viral Fusion and Regulates the Antiviral Activity of Fusion
34 Inhibitors. *Viruses* 11.
- 35 33. Deng, Y., Q. Zheng, T. J. Ketas, J. P. Moore, and M. Lu. 2007. Protein design of
36 a bacterially expressed HIV-1 gp41 fusion inhibitor. *Biochemistry* 46:4360-
37 4369.
- 38 34. Cole, J. L., and V. M. Garsky. 2001. Thermodynamics of peptide inhibitor
39 binding to HIV-1 gp41. *Biochemistry* 40:5633-5641.
- 40 35. Sia, S. K., P. A. Carr, A. G. Cochran, V. N. Malashkevich, and P. S. Kim. 2002.
41 Short constrained peptides that inhibit HIV-1 entry. *Proceedings of the National*
42 *Academy of Sciences of the United States of America* 99:14664-14669.
- 43 36. Gasteiger, E., C. Hoogland, A. Gattiker, S. e. Duvaud, M. R. Wilkins, R. D.
44 Appel, and A. Bairoch. 2005. Protein Identification and Analysis Tools on the
45 ExpASY Server. In *The Proteomics Protocols Handbook*. J. M. Walker, editor.
46 Humana Press, Totowa, NJ. 571-607.
- 47 37. Anthis, N. J., and G. M. Clore. 2013. Sequence-specific determination of protein
48 and peptide concentrations by absorbance at 205 nm. *Protein Sci* 22:851-858.
- 49
50
51
52
53
54
55
56
57
58
59
60
61
62
63
64
65

- 1
2
3
4
5
6
7
8
9
10
11
12
13
14
15
16
17
18
19
20
21
22
23
24
25
26
27
28
29
30
31
32
33
34
35
36
37
38
39
38. Sigurskjold, B. W. 2000. Exact analysis of competition ligand binding by displacement isothermal titration calorimetry. *Anal Biochem* 277:260-266.
 39. Yu, Y. B., P. L. Privalov, and R. S. Hodges. 2001. Contribution of translational and rotational motions to molecular association in aqueous solution. *Biophysical journal* 81:1632-1642.
 40. Zhou, H. X., and M. K. Gilson. 2009. Theory of free energy and entropy in noncovalent binding. *Chem Rev* 109:4092-4107.
 41. Dwyer, J. J., K. L. Wilson, D. K. Davison, S. A. Freel, J. E. Seedorff, S. A. Wring, N. A. Tvermoes, T. J. Matthews, M. L. Greenberg, and M. K. Delmedico. 2007. Design of helical, oligomeric HIV-1 fusion inhibitor peptides with potent activity against enfuvirtide-resistant virus. *Proceedings of the National Academy of Sciences of the United States of America* 104:12772-12777.
 42. Jiang, S., H. Lu, S. Liu, Q. Zhao, Y. He, and A. K. Debnath. 2004. N-substituted pyrrole derivatives as novel human immunodeficiency virus type 1 entry inhibitors that interfere with the gp41 six-helix bundle formation and block virus fusion. *Antimicrobial agents and chemotherapy* 48:4349-4359.
 43. Wang, Y., H. Lu, Q. Zhu, S. Jiang, and Y. Liao. 2010. Structure-based design, synthesis and biological evaluation of new N-carboxyphenylpyrrole derivatives as HIV fusion inhibitors targeting gp41. *Bioorg Med Chem Lett* 20:189-192.
 44. Liu, B., R. W. Joseph, B. D. Dorsey, R. A. Schiksnis, K. Northrop, M. Bukhtiyarova, and E. B. Springman. 2009. Structure-based design of substituted biphenyl ethylene ethers as ligands binding in the hydrophobic pocket of gp41 and blocking the helical bundle formation. *Bioorg Med Chem Lett* 19:5693-5697.
 45. Sofiyev, V., H. Kaur, B. A. Snyder, P. A. Hogan, R. G. Ptak, P. Hwang, and M. Gochin. 2017. Enhanced potency of bivalent small molecule gp41 inhibitors. *Bioorg Med Chem* 25:408-420.
 46. Nussinov, R., and C. J. Tsai. 2013. Allostery in disease and in drug discovery. *Cell* 153:293-305.

Figure Legends

40
41
42

Figure 1. CovNHR-C34 complex structure, gp41 domain organization and the different sequences used in this work. (a) Surface representation of the contacts between the NHR and CHR regions of covNHR-VQ (grey) and C34 (green). The contact zone of the C-terminal pocket (CTP) is represented in yellow, the amino acids that form the hydrophobic pocket (HP) are highlighted in magenta, the zone of the middle pocket (MP) is in blue and the contacts in the N-terminal pocket (NTP) in red. (b) Schematic representation of gp41 ectodomain functional regions. The residue numbers defining each region correspond to gp160 sequence numbers. FP, fusion peptide; FPPR, Fusion-peptide proximal region; NHR, N-terminal heptad repeat; DSL, disulfide-bonded loop; CHR, C-terminal heptad repeat; MPER, Membrane-proximal external region. Reference

43
44
45
46
47
48
49
50
51
52
53
54
55
56
57
58
59
60
61
62
63
64
65

1 sequences (Swiss-Prot entry sp|P03377|ENV_HV1BR) of NHR (blue) and CHR
2 (green). The interaction between the residues in C-terminal heptad repeat and N-
3 terminal heptad repeat is represented with the black dotted lines. (c) Sequences of the
4 CHR peptides used in this study. Residues of the CTP binding motif are highlighted in
5 yellow, the binding motif residues to the HP in magenta, to the MP in blue and to the
6 NTP in red.
7
8
9

10
11
12 **Figure 2.** Far UV (a-b) and Near UV (c-d) CD spectra of free covNHR proteins and 1:2
13 mixtures of the proteins with CHR peptides. The far-UV spectrum of C34 is also shown
14 in dashed pink lines. The Near UV CD spectrum of C34 is almost flat and has been
15 omitted in panels c and d for clarity. The CD signal is normalized as molar ellipticity
16 units. Protein concentrations used were 15 μ M and 40 μ M in panels (a-b) and (c-d)
17 respectively. Experiments corresponding to covNHR-VQ/C34 (continuous grey lines)
18 were taken from our previous study [26].
19
20
21
22
23
24
25
26

27 **Figure 3.** Isothermal titration calorimetry of W24N binding to covNHR-VQ at 25°C
28 (a). ITC binding isotherm shown in the bottom panel is calculated from the thermogram
29 of the upper panel. The symbols correspond to the experimental heats and the lines
30 represent the fittings using a binding model of n identical and independent sites. ITC
31 competition experiments between covNHR-VQ/N25S and W24N (b). The total
32 concentration of N25S incubated with the protein is 20 μ M (blue binding isotherm) and
33 40 μ M (green binding isotherm).
34
35
36
37
38
39
40
41

42 **Figure 4.** Thermodynamic signature of the binding of CHR peptides to covNHR-VQ
43 (a-c). Comparison of the thermodynamic binding parameters of W24N (d), W13S (e)
44 and N36N (f) to the covNHR proteins. The values have been calculated from the
45 parameters of Table 1.
46
47
48
49
50
51
52
53
54
55
56
57
58
59
60
61
62
63
64
65

Figure 2

Figure 2.

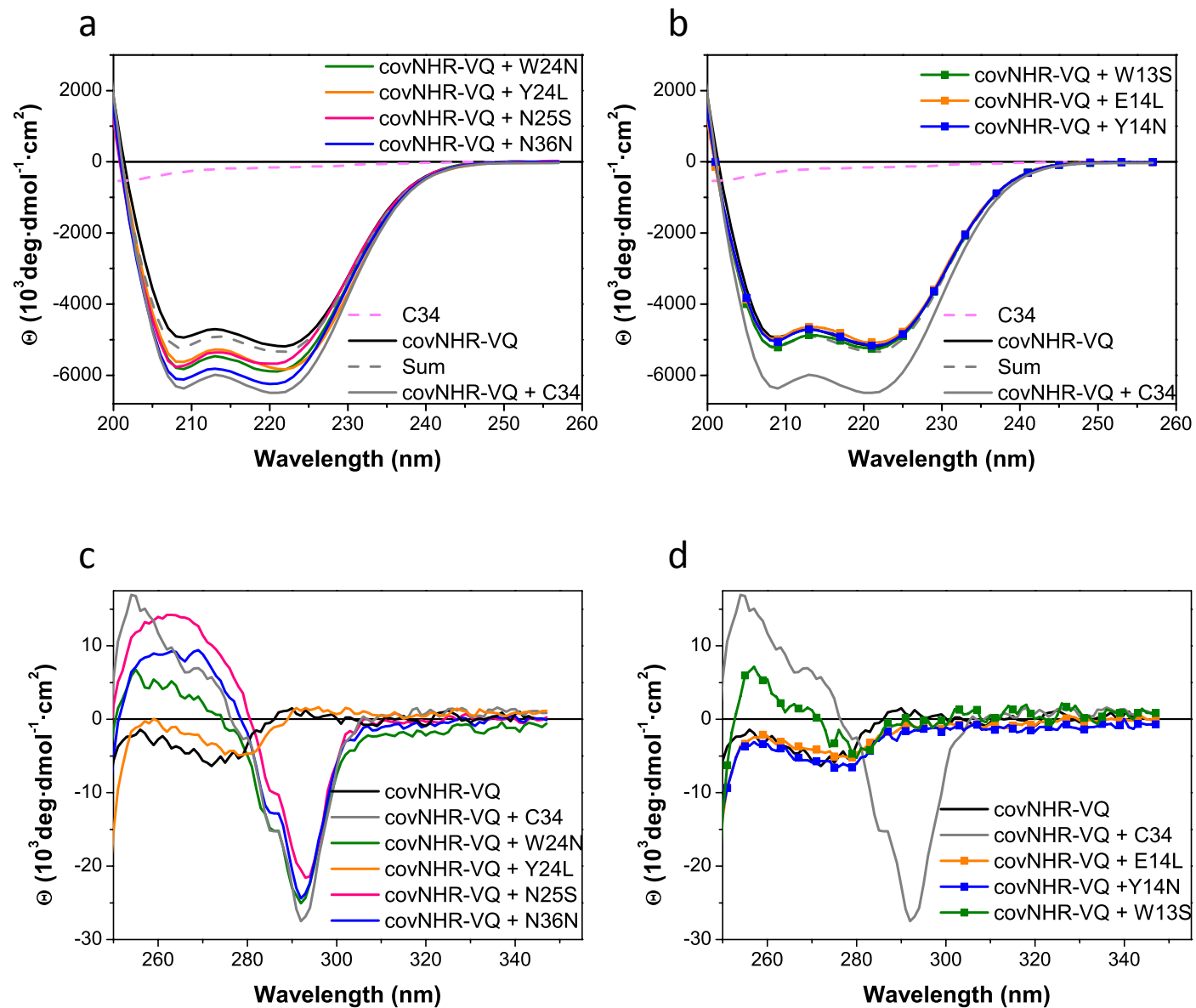


Figure 3
Figure 3.

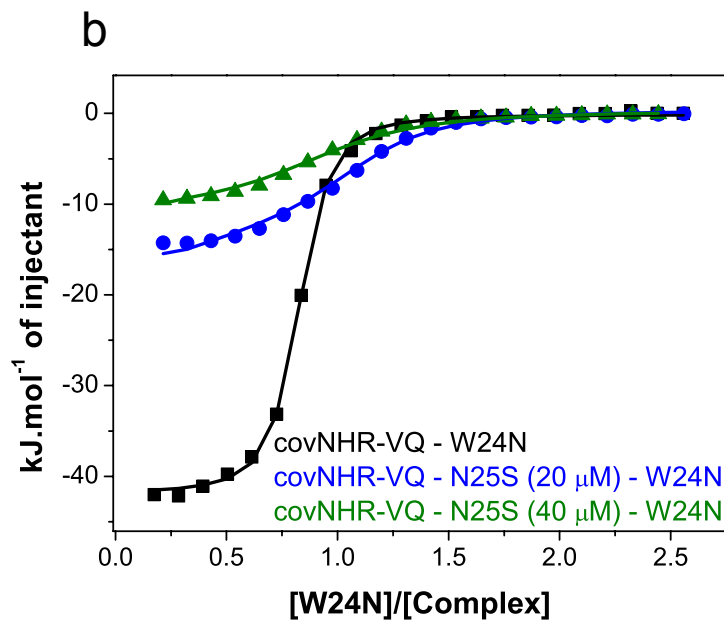
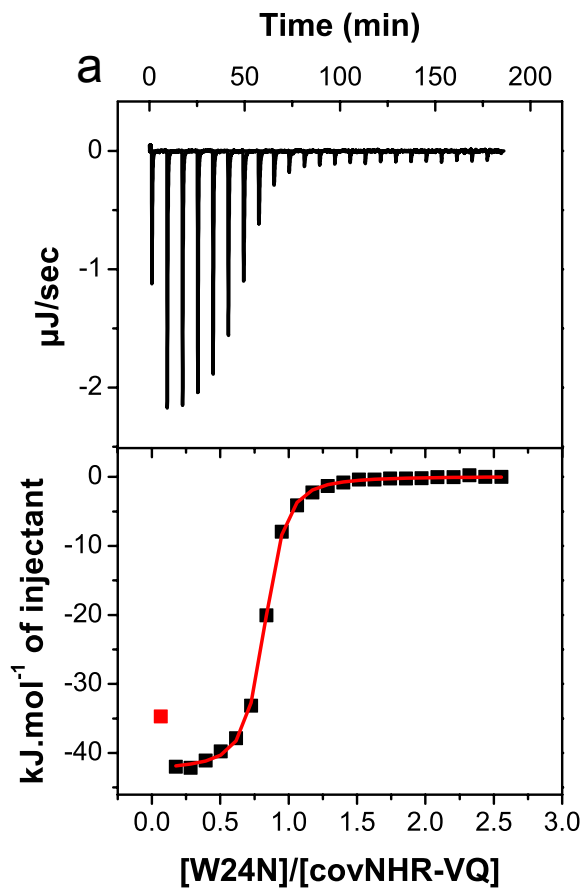
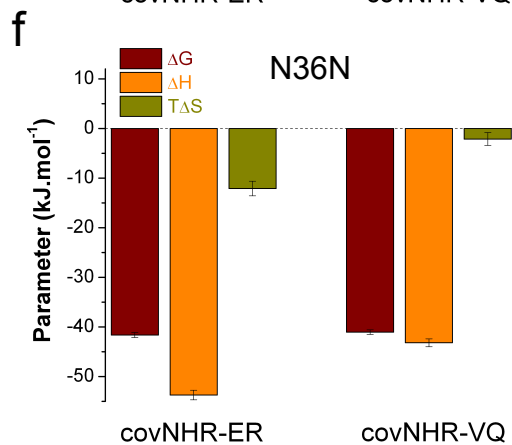
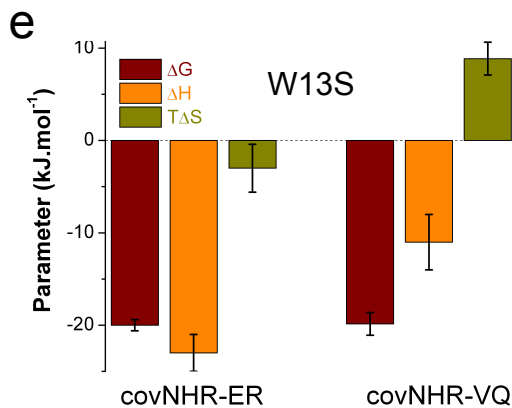
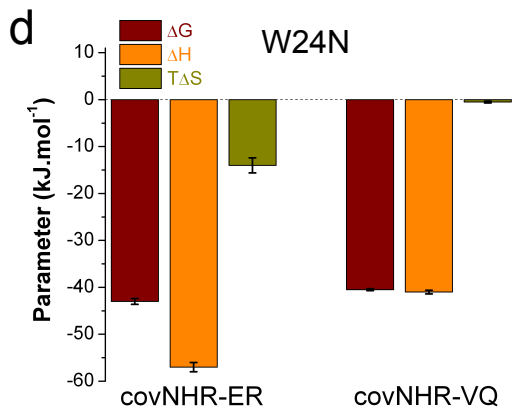
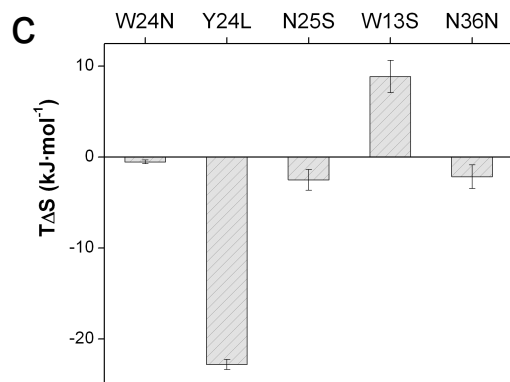
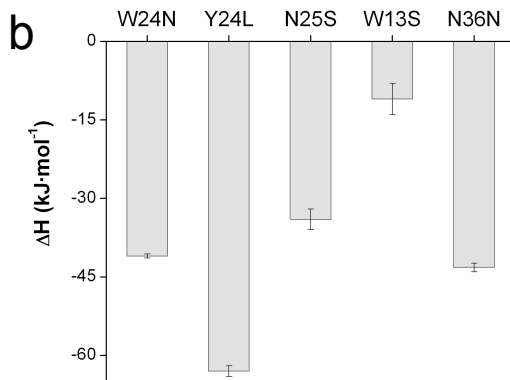
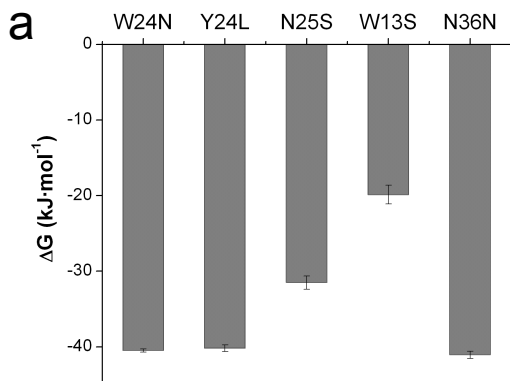


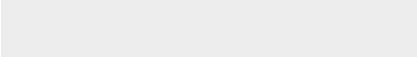
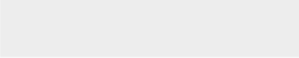
Figure 4
Figure 4.



1
2
3
4
5
6
7
8
9
10
11
12
13
14
15
16
17
18
19
20
21
22
23
24
25
26
27
28
29
30
31
32
33
34
35
36
37
38
39
40
41
42
43
44
45
46
47
48
49
50
51
52
53
54
55
56
57
58
59
60
61
62
63
64
65



Click here to access/download
Table
Table_Jurado_revised.pdf



1
2
3
4
5
6
7
8
9
10
11
12
13
14
15
16
17
18
19
20
21
22
23
24
25
26
27
28
29
30
31
32
33
34
35
36
37
38
39
40
41
42
43
44
45
46
47
48
49
50
51
52
53
54
55
56
57
58
59
60
61
62
63
64
65



Click here to access/download
Supporting File
SI_Jurado_revised.pdf

